



Structural and mechanical evolution of reactively and non-reactively sputtered Zr–Al–N thin films during annealing[☆]

P.H. Mayrhofer^{a,*}, D. Sonnleitner^b, M. Bartosik^a, D. Holec^b

^a Institute of Materials Science and Technology, Vienna University of Technology, A-1040 Vienna, Austria

^b Department of Physical Metallurgy and Materials Testing, Montanuniversität Leoben, A-8700 Leoben, Austria

ARTICLE INFO

Article history:

Received 9 October 2013

Accepted in revised form 25 January 2014

Available online 2 February 2014

Keywords:

ZrAlN

Non-reactive sputtering

Decomposition

Age-hardening

DS

ABSTRACT

The influence of reactive and non-reactive sputtering on structure, mechanical properties, and thermal stability of $Zr_{1-x}Al_xN$ thin films during annealing to 1500 °C is investigated in detail. Reactive sputtering of a $Zr_{0.6}Al_{0.4}$ target leads to the formation of $Zr_{0.66}Al_{0.34}N$ thin films, mainly composed of supersaturated cubic (c) $Zr_{1-x}Al_xN$ with small fractions of (semi-)coherent wurtzite (w) AlN domains. Upon annealing, the formation of cubic Zr-rich domains and growth of the (semi-)coherent w-AlN domains indicate spinodal-like decomposition. Loss of coherency can only be observed for annealing temperatures above 1150 °C. Following these decomposition processes, the hardness remains at the as-deposited value of ~29 GPa with annealing up to 1100 °C. Using a ceramic $(ZrN)_{0.6}(AlN)_{0.4}$ target and sputtering in Ar atmosphere allows preparing $c-Zr_{0.68}Al_{0.32}N$ coatings with a well-defined crystalline single-phase cubic structure combined with higher hardnesses of ~31 GPa. Due to the absence of (semi-)coherent w-AlN domains in the as-deposited state, which could act as nucleation sites, the decomposition process of $c-Zr_{1-x}Al_xN$ is retarded. Only after annealing at 1270 °C, the formation of incoherent w-AlN can be detected. Hence, their hardness remains very high with ~33 GPa even after annealing at 1200 °C. The study highlights the importance of controlling the deposition process to prepare well-defined coatings with high mechanical properties and thermal stability.

© 2014 The Authors. Published by Elsevier B.V. All rights reserved.

1. Introduction

Transition metal nitride thin films are used for a wide variety of applications as they combine excellent mechanical properties with high thermal stability, oxidation and corrosion resistance, and exhibit distinct optical properties [1–8]. Particularly, for machining and forming applications, $Cr_{1-x}Al_xN$ and $Ti_{1-x}Al_xN$ count to the most used coating systems. Hence many research activities concentrate on their synthesis–structure–property relations and improvements by e.g., architecture (including multilayer and superlattice design), chemical variations and alloys [9–16]. Especially the increase in oxidation resistance, due to the formation of dense Al_2O_3 layers, as well as the increase in thermal stability compared to TiN or CrN made $Ti_{1-x}Al_xN$ and $Cr_{1-x}Al_xN$ very attractive for industrial applications [14,17]. The maximum solubility of Al (x) in physical vapour deposited (PVD) metastable face centred cubic (B1, NaCl-type) phases of $Ti_{1-x}Al_xN$ and $Cr_{1-x}Al_xN$ is around $x \sim 0.66$ and ~ 0.77 , respectively. When exceeding this metastable solubility limit of

Al in the cubic structure, the formation of a hexagonal close packed (B4, wurtzite-type) phase is promoted [9,10,18–25]. The wurtzite-type (w) phase is the stable structure of AlN and exhibits lower mechanical strength and elastic constants as compared with the metastable cubic (c) counterpart [10,26]. Hence, especially for applications requiring mechanical strength and stiffness in combination with high oxidation resistance, single-phase cubic structured $Ti_{1-x}Al_xN$ and $Cr_{1-x}Al_xN$ with the highest possible Al contents are favoured. But even for such optimized coatings a major problem for $Ti_{1-x}Al_xN$ is the formation of porous TiO_2 [14], and for $Cr_{1-x}Al_xN$ the dissociation of Cr–N bonds towards Cr_2N and Cr with simultaneous release of N_2 [20,27], upon exposure to air at elevated temperatures. To overcome, or at least reduce these drawbacks, alloying concepts are developed for both systems [28–30].

$Zr_{1-x}Al_xN$ coatings are promising alternatives and have attracted already a lot of interest over the last years, due to their phase stability as well as excellent mechanical properties (like hardness and indentation modulus) and thermal stability [31–38]. Similarly to $Ti_{1-x}Al_xN$ and $Cr_{1-x}Al_xN$ also here single-phase cubic structured films with high Al-contents are favoured. *Ab initio* calculations show that cubic structured $Zr_{1-x}Al_xN$ is favourable (over hexagonal, Bk, or wurtzite, B4, structured) up to $Al/(Zr + Al)$ contents of $x \sim 0.43$ or ~ 0.5 [36,37]. For higher Al contents up to $x \sim 0.68$ the cubic B1 as well as the hexagonal Bk phase have comparable energy of formation and when exceeding

[☆] This is an open-access article distributed under the terms of the Creative Commons Attribution-NonCommercial-No Derivative Works License, which permits non-commercial use, distribution, and reproduction in any medium, provided the original author and source are credited.

* Corresponding author.

E-mail address: paul.mayrhofer@tuwien.ac.at (P.H. Mayrhofer).

$x \sim 0.68$ the wurtzite B4 phase is favoured [36]. This is in good agreement with experimental data for $\text{Zr}_{1-x}\text{Al}_x\text{N}$ exhibiting a predominant cubic structure for $x \leq 0.43$ and an at least two-phased structure (cubic and hexagonal) for $0.43 \leq x \leq 0.73$ [33,38]. Single phase cubic structured $\text{Zr}_{1-x}\text{Al}_x\text{N}$ can possess hardnesses up to ~ 46 GPa, but as soon as a wurtzite phase is present, the hardness decreases to ~ 28 GPa [25]. Especially for $\text{Zr}_{1-x}\text{Al}_x\text{N}$ coatings, exhibiting small grain sizes and amorphous-like phase contents in the as-deposited state a significant increase in hardness is obtained upon annealing [38,39]. All of these coatings were prepared by reactive PVD techniques and are generally overstoichiometric in their nitrogen content. We envision, that this is driven by the preferred formation of Zr_3N_4 -based phases [40,41] upon providing enough nitrogen. The as-deposited nano-structure of $\text{Zr}_{1-x}\text{Al}_x\text{N}$ thin films originates also from the formation of w-AlN domains (semi-)coherent to supersaturated cubic $\text{Zr}_{1-x}\text{Al}_x\text{N}$ phases [42]. Therefore, we study and compare reactively and non-reactively prepared $\text{Zr}_{1-x}\text{Al}_x\text{N}$ coatings with respect to their structure, mechanical properties, and thermal stability. To ensure the formation of a single-phase cubic structure we have used powder metallurgically prepared targets with moderate Al-contents, $\text{Zr}_{0.6}\text{Al}_{0.4}$ and $(\text{ZrN})_{0.6}(\text{AlN})_{0.4}$.

2. Experimental

$\text{Zr}_{1-x}\text{Al}_x\text{N}$ coatings were prepared reactively and non-reactively by magnetically unbalanced DC magnetron sputtering of a $\text{Zr}_{0.6}\text{Al}_{0.4}$ target in Ar-N_2 and a $(\text{ZrN})_{0.6}(\text{AlN})_{0.4}$ target in Ar glow discharges, respectively. The powder metallurgically prepared targets (150 mm in diameter and 6 mm thick, PLANSEE SE) face the substrates (MgO (100), sapphire, polished Si (100), and low-alloy steel foil) at the parallel and centred substrate holder with a distance of 55 mm [43]. Prior to the depositions, the substrates were ultrasonically precleaned in acetone and ethanol, and plasma-etched within the chamber using an $\text{Ar} +$ glow discharge with -1000 V and ~ 15 mA at a pressure of 1 Pa. Reactive deposition was conducted with a N_2 -to-total pressure ratio of $\sim 17\%$, based on pre-studies showing that here the target is in the transition between metallic and compound mode (or poisoned mode) resulting in a high deposition rate combined with a close-to-stoichiometry nitride formation of the prepared coating. For both deposition types (reactive and non-reactive) the total pressure was 0.4 Pa, the sputter power density was 3 W/cm^2 , the substrate temperature was 500°C , and the deposition time was 45 min. The applied substrate bias potential of -60 V resulted in a substrate current I_s of ~ 170 mA (157 mm diameter substrate holder) for both deposition conditions.

Biaxial film stress measurements were obtained by the cantilever beam method using the modified Stoney equation [44]. Composition and morphology of the thin films were studied by energy dispersive X-ray analysis (EDX) and scanning electron microscope (SEM) using an Oxford Instruments INCA EDX unit integrated to a Zeiss Evo 50 SEM. Quantification is obtained by means of a $\text{Zr}_{0.71}\text{Al}_{0.29}\text{N}_{0.84}$ thin film standard, calibrated using elastic recoil detection analyses. Structure and phase analyses were carried out by X-ray diffraction (XRD) with a Bruker-AXS D8 in Bragg–Brentano configuration equipped with a $\text{Cu-K}\alpha$ radiation source. Lattice parameters are obtained using Rietveld analysis [45]. The coherently diffracting domain size d and the microstrains ε (strains of second and third order) were evaluated from the XRD powder patterns applying the Williamson–Hall analysis [46,47].

Hardness (H) and modulus of indentation (E) of the coatings (on MgO substrates) were evaluated from load–displacement curves obtained by a computer controlled nanoindenter (Berkovich diamond tip, Ultra Micro Indentation System UMIS, Fischer–Cripps Laboratories) using the Oliver and Pharr method [48]. The maximum normal loads were between 30 and 15 mN in steps of 1 mN to ensure that the maximum indentation depth was below 10% of the film thickness.

Differential scanning calorimetry (DSC) in combination with thermo-gravimetric analysis (TGA) was performed with freestanding coating material using a SETSYS Evolution TMA (Setaram Instrumentation) calorimeter. To avoid substrate interference during this study, the low alloy steel foil substrates were chemically removed with diluted nitric acid. The DSC–TGA measurements were performed in He atmosphere up to 1500°C using a heating rate of 23 K/min and a cooling rate of 50 K/min .

Vacuum annealing of the coatings on MgO and sapphire substrates was carried out in a HTM-Reetz vacuum furnace (pressure below 0.1 mPa) at temperatures between 600 and 1200°C in steps of 100°C for nanoindentation. A heating rate of 20 K/min and a holding time of 20 min at the given temperature were chosen. Additionally, powdered freestanding coating material (as used for the DSC–TGA measurements) was annealed at selected temperatures where distinct DSC reactions occur. Prior and after these annealing treatments the coatings were again analysed by XRD.

3. Results and discussion

The reactively (r) and non-reactively (nr) sputtered nitride films have nitrogen contents of 47.9 ± 1.8 and 46.0 ± 1.2 at.% and Al/(Al + Zr) ratios of $x = 0.34 \pm 0.03$ and 0.32 ± 0.01 , respectively. Consequently, their Al-contents are slightly lower as in the targets used. As XRD suggests only for a single-phase face centred cubic ZrN based structure, Fig. 1, we refer to our coatings with r- $\text{Zr}_{0.66}\text{Al}_{0.34}\text{N}$ and nr- $\text{Zr}_{0.68}\text{Al}_{0.32}\text{N}$. The XRD peaks of the reactively sputtered coatings are broader having an integral width Γ_{200} of the (200) peak of $\sim 2.7^\circ$, whereas $\Gamma_{200} \sim 1.3^\circ$ for nr- $\text{Zr}_{0.68}\text{Al}_{0.32}\text{N}$. In combination with the higher background level, the broad XRD peaks for r- $\text{Zr}_{0.66}\text{Al}_{0.34}\text{N}$ suggest for the presence of an additional phase, similar to the observations made for $\text{Ti}_{1-x}\text{Al}_x\text{N}$ [52]. A comparable XRD pattern with an increased background level is also presented for single-phase face centred cubic $\text{Zr}_{1-x}\text{Al}_x\text{N}$ with $x = 0.15, 0.35, 0.38$, and 0.43 [33,49]. Recent studies showed that this can be due to the formation of (semi-)coherent w-AlN domains to c- $\text{Zr}_{1-x}\text{Al}_x\text{N}$ during film growth, leading to self-organized nanostructures [42]. We envision that a corresponding (semi-)coherent phase formation is responsible for the broad XRD peaks of the reactively prepared coatings. Their coherently diffracting domain size d is ~ 8 nm in comparison to 36 nm for nr- $\text{Zr}_{0.68}\text{Al}_{0.32}\text{N}$. The lattice parameters a , obtained from Rietveld analysis, are 4.502 \AA for r- $\text{Zr}_{0.66}\text{Al}_{0.34}\text{N}$ and 4.491 \AA for nr- $\text{Zr}_{0.68}\text{Al}_{0.32}\text{N}$. These are in excellent agreement to the *ab initio* obtained value of 4.498 \AA for $\text{Zr}_{0.67}\text{Al}_{0.33}\text{N}$ [36] and experimentally obtained value of 4.483 \AA for $\text{Zr}_{0.65}\text{Al}_{0.35}\text{N}$ [38]. The larger crystallite size d in combination with the smaller lattice parameter a for nr- $\text{Zr}_{0.68}\text{Al}_{0.32}\text{N}$ indicates that here the formation of (semi-)coherent w-AlN domains is not as pronounced (or even completely suppressed) during growth.

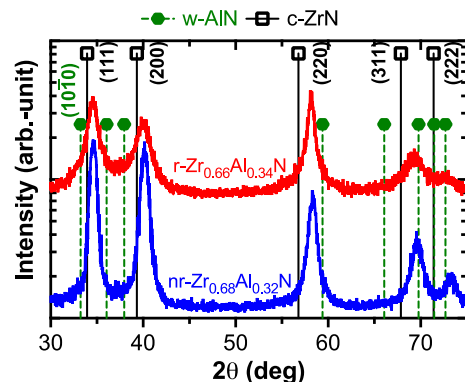


Fig. 1. XRD patterns from reactively prepared r- $\text{Zr}_{0.66}\text{Al}_{0.34}\text{N}$ and non-reactively prepared nr- $\text{Zr}_{0.68}\text{Al}_{0.32}\text{N}$ coatings in their as-deposited state.

Hence, more Al needs to be solved within the cubic lattice leading to a smaller lattice parameter a [36].

The reactive deposition rate is 100 nm/min which is higher than the non-reactive deposition rate of 74 nm/min, leading to ~ 4.4 and ~ 3.3 μm thick coatings for the deposition time of 45 min. These results confirm that for ideal N_2 -to-total pressure ratios the poisoning behaviour of the $\text{Zr}_{0.6}\text{Al}_{0.4}$ target can be minimized guaranteeing a metallic deposition mode and the preparation of an almost stoichiometric nitride. As a result of the stronger nitride bindings in the ceramic $(\text{ZrN})_{0.6}(\text{AlN})_{0.4}$ target, the non-reactive sputter rate is lower as compared with the reactive sputter rate using an ideal N_2 -to-total pressure ratio and a metallic $\text{Zr}_{0.6}\text{Al}_{0.4}$ target. Both coatings exhibit an extremely dense growth morphology and surface roughnesses of $R_a < 10$ nm. Their nearly featureless as-deposited fracture cross sections are presented later when discussing the thermal stability. The lower deposition rate at a comparable substrate current ($I_s \sim 170$ mA, see Experimental) suggests that the average delivered energy to the non-reactively grown film is higher as compared to the reactively grown film. Furthermore, reactive and non-reactive sputtering provides different species for film-growth, especially with respect to nitrogen. Together, these effects can lead to the development of a well defined crystalline cubic $\text{Zr}_{1-x}\text{Al}_x\text{N}$ phase for the non-reactively prepared coating, whereas the reactively prepared coating exhibits also w-AlN domains, presumably (semi-)coherent to the cubic solid solution $\text{Zr}_{1-x}\text{Al}_x\text{N}$ phase.

The hardness H is 28.6 ± 0.6 GPa and the indentation modulus E is 347 ± 9 GPa for the reactively prepared coating. Slightly higher values with $H = 31.1 \pm 0.9$ GPa and $E = 398 \pm 14$ GPa are obtained for nr- $\text{Zr}_{0.68}\text{Al}_{0.32}\text{N}$. Both coatings have compressive stresses of -0.7 ± 0.2 GPa, obtained from cantilever beam method. The larger indentation modulus for the non-reactive deposition confirms the XRD observations and is consistent with atomistic simulations showing that the elastic constants C_{11} , C_{12} , and C_{44} at metal grain boundaries are only about 70% of those of the grain interior [50]. Thus, the elastic modulus is expected to decrease with decreasing grain size, as the boundary fraction decreases.

The DSC measurements of both coatings in inert atmosphere exhibit pronounced exothermic features in the temperature range between 500 and 1500 $^{\circ}\text{C}$ (Fig. 2a). The peak temperatures of the major exothermic reaction are ~ 1000 $^{\circ}\text{C}$ and ~ 1075 $^{\circ}\text{C}$ for the reactively and non-reactively prepared coatings, respectively. For temperatures up to 1000 $^{\circ}\text{C}$ the exothermic heatflow is more pronounced for r- $\text{Zr}_{0.66}\text{Al}_{0.34}\text{N}$ than for nr- $\text{Zr}_{0.68}\text{Al}_{0.32}\text{N}$, indicating more pronounced

reactions. Contrary, for temperatures above 1300 $^{\circ}\text{C}$ the nr- $\text{Zr}_{0.68}\text{Al}_{0.32}\text{N}$ coating exhibits a more pronounced DSC feature. The combined TGA measurements, Fig. 2b, furthermore show that almost no mass-loss can be detected for r- $\text{Zr}_{0.66}\text{Al}_{0.34}\text{N}$ and nr- $\text{Zr}_{0.68}\text{Al}_{0.32}\text{N}$. The mass loss of $\sim 0.08\%$ in the temperature range between 1400 and 1500 $^{\circ}\text{C}$ corresponds to a loss of only ~ 0.5 at.% N, indicating that both nitrides are very stable with respect to nitrogen release. Complementary XRD measurements of samples annealed to temperatures 850, 1150, 1270, and 1500 $^{\circ}\text{C}$ —slightly beyond distinct DSC features—allow identifying the major contributions to these reactions.

Annealing of the reactively prepared coatings to $T_a = 850$ $^{\circ}\text{C}$ results in a small shift of the XRD peak positions to lower diffraction angles (Fig. 3a). The left-hand shoulder formation of the cubic XRD peaks indicates decomposition of the supersaturated cubic r- $\text{Zr}_{0.66}\text{Al}_{0.34}\text{N}$ matrix to form c-ZrN. No c-AlN can be detected, in contrast to $\text{Ti}_{1-x}\text{Al}_x\text{N}$ coatings [12], suggesting that (semi-)coherent w-AlN phases are formed, or—if already present in the as-deposited state—grow. Annealing to 1150 $^{\circ}\text{C}$ leads—on the expense of the supersaturated matrix—to a pronounced increase in intensity of the c-ZrN peaks and clearly separated w-AlN peaks, see the additional reflexes at $2\theta = 36.0$ and 37.9° in Fig. 3a. Hence, the decomposition process is nearly completed, in agreement to the DSC investigations showing a decline from the peak of the pronounced exothermic feature at this temperature. Upon further annealing, the XRD peaks for c-ZrN and w-AlN become even more distinct, suggesting completed phase separation, recrystallization, and grain growth.

The thermal stability of non-reactively prepared coatings is somehow different, as already suggested by DSC. Annealing to 850 $^{\circ}\text{C}$ only leads to a minor shift of the nr- $\text{Zr}_{0.68}\text{Al}_{0.32}\text{N}$ XRD peaks to smaller diffraction angles without indications for a shoulder formation (Fig. 3b). Annealing to 1150 and 1270 $^{\circ}\text{C}$ causes a further shift of the major cubic peaks to meet the position of c-ZrN and here especially the $(10\bar{1}0)$ w-AlN peak can be seen as it has the highest relative intensity according to [51]. In combination with the relatively broad XRD peaks at the c-ZrN position this suggests the formation of w-AlN domains. For $T_a = 1500$ $^{\circ}\text{C}$, the XRD peaks for c-ZrN and w-AlN are well defined suggesting that the exothermic DSC feature between 1300 and 1500 $^{\circ}\text{C}$ originates from the formation of crystalline incoherent w-AlN. We speculate, that during the early stages of the supersaturated cubic $\text{Zr}_{1-x}\text{Al}_x\text{N}$ decomposition, AlN forms (semi-)coherent to cubic planes. The $(111)_c - \text{ZrN} \parallel (0001)_w - \text{AlN}$ Blackburn relationship exhibits a mismatch of $\sim 4\%$. For higher temperatures, where further recovery, relaxation, and recrystallization effects are promoted—leading to breaking of the (semi-)coherency—distinct w-AlN XRD peaks, separated

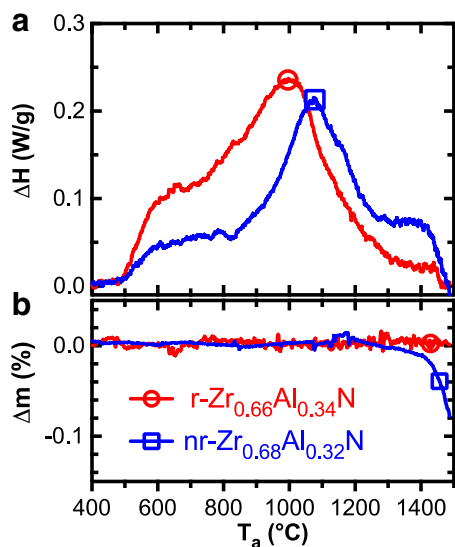


Fig. 2. (a) DSC spectra and (b) combined TGA spectra obtained during heating in He atmosphere of as-deposited reactively and non-reactively prepared $\text{Zr}_{1-x}\text{Al}_x\text{N}$ coatings (r- $\text{Zr}_{0.66}\text{Al}_{0.34}\text{N}$ and nr- $\text{Zr}_{0.68}\text{Al}_{0.32}\text{N}$).

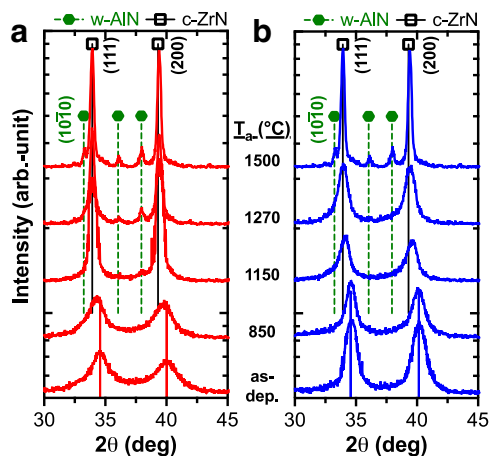


Fig. 3. XRD patterns from (a) reactively prepared r- $\text{Zr}_{0.66}\text{Al}_{0.34}\text{N}$ and (b) non-reactively prepared nr- $\text{Zr}_{0.68}\text{Al}_{0.32}\text{N}$ coatings in their as-deposited state and after annealing in vacuum at T_a for 20 min. The XRD peak positions for bulk c-ZrN and w-AlN [51] are indicated by open squares and full hexagons, respectively.

from the c-ZrN XRD peaks, can be detected. For the reactively prepared coatings this occurs at lower temperatures of $T_a \sim 1150$ °C (see Fig. 3b). We propose that here the already as-deposited present (semi-)coherent w-AlN domains act as nuclei promoting decomposition of the supersaturated matrix and growth of w-AlN crystallites. This is in agreement to DSC showing more pronounced exothermic reactions up to ~ 1100 °C for r-Zr_{0.66}Al_{0.34}N than for nr-Zr_{0.68}Al_{0.32}N.

The overall structural evolution of the reactively and non-reactively prepared coatings during annealing to 1500 °C is summarized in Fig. 4 by the microstrains ε , the lattice parameters a , and the crystallite size d , obtained from the (111), (200), (220), (311), and (222) cubic XRD peaks. As mentioned earlier during discussing the XRD patterns, there is a left-hand shoulder formation of the cubic r-Zr_{0.66}Al_{0.34}N XRD peaks indicating the formation of c-ZrN for $T_a = 850$ °C. Due to these newly formed domains, the usually pronounced increase of d with increasing T_a above the deposition temperature [53] is partly compensated. Further annealing results in a steady increase in d and decrease in ε with T_a , Fig. 4a, indicative for grain growth processes and recovery of second and third order strains. This is different to the behaviour of nr-Zr_{0.68}Al_{0.32}N, which exhibits almost unchanged microstrain ε with T_a up to 1270 °C. Also the crystallite domain size essentially remains at the as-deposited value of ~ 36 nm for T_a up to 1270 °C. Only for higher temperatures, ε significantly decreases (to zero) and d increases to ~ 65 nm, meeting the value of r-Zr_{0.66}Al_{0.34}N at $T_a = 1500$ °C (Fig. 4a).

The lattice parameter a of the major cubic phase within the coatings gradually increases with T_a towards the value for c-ZrN ($a = 4.578$ Å), Fig. 4b. The latter is obtained for r-Zr_{0.66}Al_{0.34}N with $T_a \geq 1100$ °C and for nr-Zr_{0.68}Al_{0.32}N with $T_a \geq 1270$ °C. At these temperatures, also w-AlN could be detected by XRD (Fig. 3). Whereas the reactively prepared coating exhibits already strongly reduced microstrains ($\varepsilon \sim 0\%$), these are still very high for the non-reactively prepared coatings, even at the higher temperature of 1270 °C. The nearly perfect match of the lattice parameter with c-ZrN, in combination to high microstrains ε and almost no detectable w-AlN XRD peaks, is indicative for (semi-)coherency between cubic ZrN and wurtzite AlN domains. The delayed increase in a and d , and delayed decrease in ε with T_a for nr-Zr_{0.68}Al_{0.32}N as compared to r-Zr_{0.66}Al_{0.34}N can be explained by their as-deposited structure. In reactively prepared coatings,

(semi-)coherent w-AlN domains are present already in the as-deposited state, which can act as nucleation sites for further decomposition of the supersaturated c-Zr_{1-x}Al_xN phase. This is not the case for their non-reactively prepared counterparts, and hence, decomposition of c-Zr_{1-x}Al_xN and formation of w-AlN are retarded.

Based on the DSC and XRD studies we can conclude that supersaturated c-Zr_{1-x}Al_xN can undergo spinodal-like decomposition to form coherent Zr-rich cubic domains and presumably (semi-)coherent w-AlN domains. With proceeding annealing treatment these domains transform towards their incoherent stable phases c-ZrN and w-AlN. We envision that especially the formation of (semi-)coherent w-AlN domains corresponds to the formation of Guinier-Preston zones in Al-alloys [54,55].

The increased thermal stability of the non-reactively prepared coating is also proven by SEM fracture cross sections after annealing r-Zr_{0.66}Al_{0.34}N to 1100 °C and nr-Zr_{0.68}Al_{0.32}N to 1200 °C, Fig. 5a and b, showing their upper surface-near part. We have added fracture cross sections in their as-deposited state for comparison. The reactively prepared coating exhibits the development of small equiaxed grains upon annealing to 1100 °C. This cannot be observed for the non-reactively prepared counterpart, showing a similar smooth and nearly featureless fracture morphology as in the as-deposited state, even after annealing at 1200 °C. This is in agreement to DSC and XRD studies, suggesting a higher thermal stability for non-reactively prepared coatings as compared to their reactively prepared counterparts.

The different structural development of the reactively and non-reactively prepared coatings upon annealing leads also to a different hardness development. The hardness of r-Zr_{0.66}Al_{0.34}N stays within the error of measurement at the as-deposited value of ~ 28 GPa upon annealing to 1100 °C (Fig. 6). Contrary, the non-reactively prepared coating nr-Zr_{0.68}Al_{0.32}N shows a steady increase in H from the as-deposited value of ~ 31 GPa to 33 GPa with increasing T_a to 900–1100 °C. Even after annealing at 1200 °C, the hardness of this coating (on sapphire) is 32.9 ± 1.7 GPa. The relatively high hardness for both coatings after annealing to 1100 °C can be related to their extremely high structural thermal stability, where small fractions of incoherent w-AlN can only be detected after annealing r-Zr_{0.66}Al_{0.34}N to 1150 °C and nr-Zr_{0.68}Al_{0.32}N to 1270 °C.

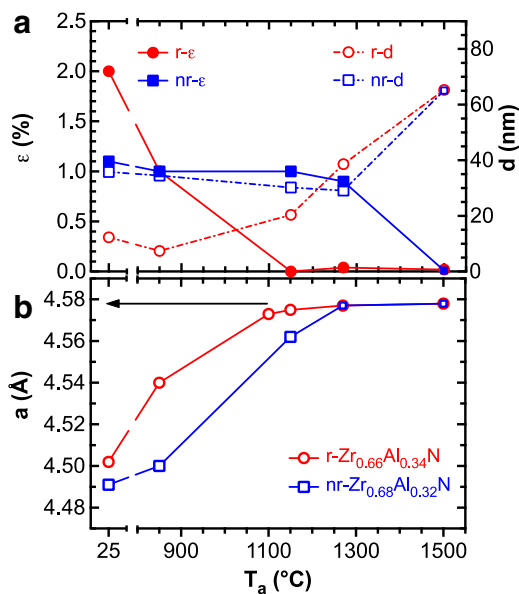


Fig. 4. (a) Microstrains ε and crystallite sizes d and (b) lattice parameters a of the major cubic phase within r-Zr_{0.66}Al_{0.34}N and nr-Zr_{0.68}Al_{0.32}N as a function of T_a . For comparison the lattice parameter $a_0 = 4.578$ Å of bulk c-ZrN [51] is indicated by an arrow.

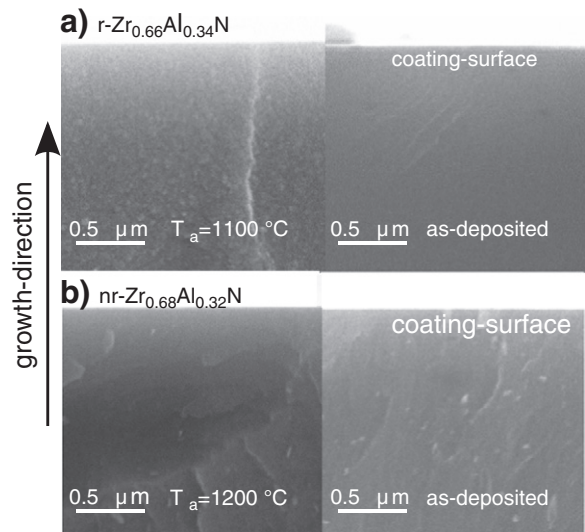


Fig. 5. Fracture cross section SEM images showing the surface-near part of (a) r-Zr_{0.66}Al_{0.34}N after annealing at 1100 °C and of (b) nr-Zr_{0.68}Al_{0.32}N after annealing at 1200 °C. Fracture cross section SEM images of their as-deposited state are given for comparison on their right side.

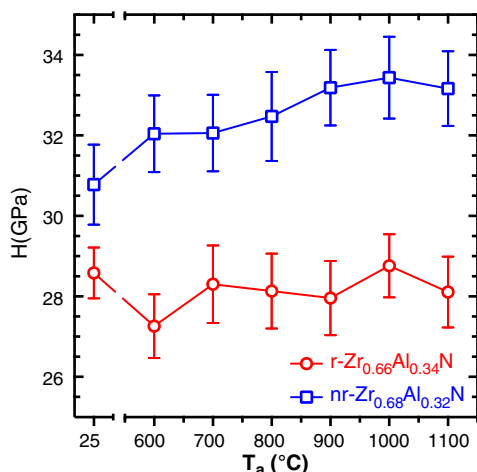


Fig. 6. Hardness H of reactively prepared $r\text{-Zr}_{0.66}\text{Al}_{0.34}\text{N}$ and non-reactively prepared $\text{nr-Zr}_{0.68}\text{Al}_{0.32}\text{N}$ after annealing in vacuum at T_a for 20 min.

4. Conclusions

Based on different growth conditions between reactive and non-reactive depositions, the structure, mechanical properties, as well as thermal stability of $\text{Zr}_1 - x\text{Al}_x\text{N}$ coatings are different. Non-reactive sputtering of a ceramic $(\text{ZrN})_{0.6}(\text{AlN})_{0.4}$ target in Ar atmosphere results in the formation of a $\text{nr-Zr}_{0.68}\text{Al}_{0.32}\text{N}$ coating. A comparable chemical composition, $r\text{-Zr}_{0.66}\text{Al}_{0.34}\text{N}$, is obtained when using reactive sputtering of a $\text{Zr}_{0.6}\text{Al}_{0.4}$ target in a mixed Ar/N_2 atmosphere. However, the lower deposition rate of 74 nm/min for $\text{nr-Zr}_{0.68}\text{Al}_{0.32}\text{N}$ as compared to 100 nm/min for $r\text{-Zr}_{0.66}\text{Al}_{0.34}\text{N}$ suggests that the average delivered energy during film-growth is higher, respectively, as for both depositions comparable substrate currents are obtained. The combination with the different species provided leads to the development of a well defined crystalline cubic $\text{Zr}_1 - x\text{Al}_x\text{N}$ phase in $\text{nr-Zr}_{0.68}\text{Al}_{0.32}\text{N}$, whereas also $w\text{-AlN}$ domains—presumably (semi-)coherent to the cubic solid solution $\text{Zr}_1 - x\text{Al}_x\text{N}$ phase—are present in $r\text{-Zr}_{0.66}\text{Al}_{0.34}\text{N}$. These pre-existing $w\text{-AlN}$ domains can act as nucleation sites promoting the decomposition of the supersaturated $c\text{-Zr}_1 - x\text{Al}_x\text{N}$ phase towards their stable constituents $c\text{-ZrN}$ and $w\text{-AlN}$ during thermal annealing. This is not the case for $\text{nr-Zr}_{0.68}\text{Al}_{0.32}\text{N}$ coatings, requiring to overcome the nucleation barrier. Hence, thermal decomposition is retarded with respect to their reactively prepared counterparts. We propose that the phase separation of our $\text{Zr}_1 - x\text{Al}_x\text{N}$ coatings towards their stable constituents $c\text{-ZrN}$ and $w\text{-AlN}$ follows a spinodal-like decomposition process, via the formation of coherent cubic Zr-rich and (semi-)coherent $w\text{-AlN}$ domains. This is especially valid for the non-reactively prepared coating, as here no pre-existing $w\text{-AlN}$ nuclei are present. Based on this, the hardness of $\text{nr-Zr}_{0.68}\text{Al}_{0.32}\text{N}$ is with ~33 GPa above that of $r\text{-Zr}_{0.66}\text{Al}_{0.34}\text{N}$ with ~28 GPa, after annealing between 900 and 1100 °C. These extremely high hardnesses for both coatings are based on their high structural stability. First indications, by XRD, for the formation of incoherent $w\text{-AlN}$ phases can be detected for $r\text{-Zr}_{0.66}\text{Al}_{0.34}\text{N}$ after annealing at 1150 °C and for $\text{nr-Zr}_{0.68}\text{Al}_{0.32}\text{N}$ after annealing at 1270 °C.

The results clearly show that by controlling the as-deposited structure of $\text{Zr}_1 - x\text{Al}_x\text{N}$ coatings, high mechanical strength and thermal stability can be achieved for the same composition.

Acknowledgements

This work was supported by the START project (project no. Y371) of the Austrian Science Fund (FWF).

References

- [1] L. Hultman, Vacuum 57 (2000) 1–30.
- [2] O. Knotek, W.D. Münz, T. Leyendecker, J. Vac. Sci. Technol. A 5 (1987) 2173–2180.
- [3] P.H. Mayrhofer, C. Mitterer, L. Hultman, H. Clemens, Prog. Mater. Sci. 51 (2006) 1032–1114.
- [4] E. Budke, J. Krempel-Hesse, H. Maidhof, H. Schüssler, Surf. Coat. Technol. 112 (1999) 108–113.
- [5] C. Mitterer, P.H. Mayrhofer, W. Waldhauser, E. Kelesoglu, P. Losbichler, Surf. Coat. Technol. 108–109 (1998) 230–235.
- [6] A. Hörling, L. Hultman, M. Odén, J. Sjölen, L. Karlsson, Surf. Coat. Technol. 191 (2005) 384–392.
- [7] O. Knotek, F. Löffler, G. Krämer, Surf. Coat. Technol. 54–55 (1992) 241–248.
- [8] R. Constantin, B. Miremad, Surf. Coat. Technol. 120–121 (1999) 728–733.
- [9] A. Kimura, H. Hasegawa, K. Yamada, T. Suzuki, Surf. Coat. Technol. 120–121 (1999) 438–441.
- [10] P.H. Mayrhofer, D. Music, J.M. Schneider, J. Appl. Phys. 100 (2006) 094906.
- [11] Y. Makino, ISIJ Int. 38 (1998) 25.
- [12] P.H. Mayrhofer, A. Hörling, L. Karlsson, J. Sjölen, T. Larsson, C. Mitterer, L. Hultman, Appl. Phys. Lett. 83 (10) (2003) 2049.
- [13] A. Hörling, L. Hultman, M. Odén, J. Sjölen, L. Karlsson, J. Vac. Sci. Technol. A 20 (5) (2002) 1815–1823.
- [14] S. PalDey, S.C. Deevi, Mater. Sci. Eng. A 342 (1–2) (2002) 58–79.
- [15] L. Chen, M. Moser, Y. Du, P.H. Mayrhofer, Thin Solid Films 517 (2009) 6635–6641.
- [16] A.E. Santana, A. Karimi, V.H. Derflinger, A. Schütze, Thin Solid Films 17 (2004) 689–696.
- [17] A.E. Reiter, C. Mitterer, B. Sartory, J. Vac. Sci. Technol. A 25 (2007) 711.
- [18] M. Zhou, Y. Makino, M. Nose, K. Nogi, Thin Solid Films 339 (1999) 203–208.
- [19] A. Kimura, H. Hasegawa, J. Mater. Sci. Lett. 19 (2000) 601–602.
- [20] P.H. Mayrhofer, H. Willmann, A.E. Reiter, Surf. Coat. Technol. 202 (2008) 4935–4938.
- [21] A.E. Reiter, V.H. Derflinger, B. Hanselmann, T. Bachmann, B. Sartory, Surf. Coat. Technol. 200 (2005) 2114–2122.
- [22] M. Kawate, A. Kimura, T. Suzuki, J. Vac. Sci. Technol. A 20 (5) (2002) 569–572.
- [23] P.H. Mayrhofer, D. Music, Th. Reeswinkel, H.-G. Fuß, J.M. Schneider, Acta Mater. 56 (11) (2008) 2469–2475.
- [24] A. Sugishima, H. Kajioka, Y. Makino, Surf. Coat. Technol. 97 (1997) 590–594.
- [25] Y. Makino, M. Mori, S. Miyake, K. Saito, K. Asami, Surf. Coat. Technol. 193 (2005) 219–222.
- [26] N.E. Christensen, I. Gorczyca, Phys. Rev. B 7 (1993) 4307–4314.
- [27] P.H. Mayrhofer, H. Willmann, L. Hultman, C. Mitterer, J. Phys. D: Appl. Phys. 41 (2008) 155316.
- [28] D. Holec, L. Zhou, R. Rachbauer, P.H. Mayrhofer, in: J. Morin, J.M. Pelletier (Eds.), Density Functional Theory: Principles, Applications and Analysis, Series: Physics Research and Technology Nova Science Publishers Inc., ISBN: 978-1-62417-954-9, 2013, pp. 259–284.
- [29] D. Holec, L. Zhou, R. Rachbauer, P.H. Mayrhofer, J. Appl. Phys. 113 (2013) 113510.
- [30] P.H. Mayrhofer, R. Rachbauer, F. Rovere, David Holec, J.M. Schneider, in: D. Cameron (Ed.), Comprehensive Material Processing Technology, Elsevier, 2014, pp. 01–33, (doi: 10.1016/B978-0-08-096532-1.00423-4).
- [31] J.-L. Ruan, J.-L. Huang, J.S. Chen, D.-F. Li, Surf. Coat. Technol. 200 (2005) 1652–1658.
- [32] R. Franz, M. Lechthaler, C. Polzer, C. Mitterer, Surf. Coat. Technol. 206 (8–9) (2012) 2337–2345.
- [33] R. Lamni, R. Sanjinés, F. Lévy, Thin Solid Films 478 (2005) 170–175.
- [34] R. Lamni, R. Sanjinés, M. Parlinska-Wojtan, A. Karimi, F. Lévy, J. Vac. Sci. Technol. A 23 (2005) 593.
- [35] H. Klostermann, F. Fietzke, T. Modes, O. Zywitzki, Rev. Adv. Mater. Sci. 15 (2007) 33–37.
- [36] D. Holec, R. Rachbauer, L. Chen, L. Wang, D. Luef, P.H. Mayrhofer, Surf. Coat. Technol. 206 (2011) 1698–1704.
- [37] S.H. Sheng, R.F. Zhang, S. Veprek, Acta Mater. 56 (2008) 968–976.
- [38] R. Sanjinés, C.S. Sandu, R. Lamni, F. Lévy, Surf. Coat. Technol. 200 (2006) 6308–6312.
- [39] L. Rogström, L.J.S. Johnson, M.P. Johansson, M. Ahlgren, L. Hultman, M. Odén, Scripta Mater. 62 (2010) 739–741.
- [40] H. Benia, M. Guemmaz, G. Schmerber, A. Mosser, J.-C. Parlebas, Appl. Surf. Sci. 200 (2002) 231–238.
- [41] M. Chhowalla, H.E. Unalan, Nat. Mater. 1338 (2005) 1–6.
- [42] N. Ghafoor, L.J.S. Johnson, D.O. Klenov, J. Demeulemeester, P. Desjardins, I. Petrov, L. Hultman, M. Odén, APL Mater. 1 (2013) 022105.
- [43] P.H. Mayrhofer, M. Geier, C. Löcker, L. Chen, Int. J. Mater. Res. 100 (2009) 152–158.
- [44] J.D. Wilcock, D.S. Campbell, Thin Solid Films 3 (1969) 3–12.
- [45] H.M. Rietveld, J. Appl. Crystallogr. 2 (1969) 65.
- [46] G.K. Williamson, W.H. Hall, Acta Metall. 1 (1953) 22.
- [47] E.J. Mittemeijer, U. Welzel, Z. Kristallogr. 223 (2008) 552.
- [48] W.C. Oliver, G.M. Pharr, J. Mater. Res. 7 (1992) 1564–1583.
- [49] L. Rogström, M.P. Johansson, N. Ghafoor, L. Hultman, M. Odén, J. Vac. Sci. Technol. A 30 (2012) 031504.
- [50] M.D. Kluge, D. Wolf, J.F. Lutsko, S.R. Phillpot, J. Appl. Phys. 67 (1990) 2370–2380.
- [51] Powder Diffraction File, Cards 25-1133 for $w\text{-AlN}$ and 35-0753 for $c\text{-ZrN}$, JCPDS-International Center for Diffraction Data, Swarthmore, 2001.
- [52] D. Rafaja, C. Wüstefeld, M. Motylenko, C. Schimpf, T. Barsukova, M.R. Schwarz, E. Kroke, Chem. Soc. Rev. 41 (15) (2012) 5081–5101.
- [53] P.H. Mayrhofer, M. Stoiber, C. Mitterer, Scripta Mater. 53 (2005) 241–245.
- [54] A. Guinier, Nature 142 (1938) 569–570.
- [55] G.P. Preston, Nature 142 (1938) 570–570.